ChemPubSoc Europe

DOI: 10.1002/slct.201601806

Chemistry SELECT Full Papers

Materials Science inc. Nanomaterials & Polymers

Structuring of Alkyl-Triazole Bridged Silsesquioxanes

S. C. Nunes,*[a, b] G. Toquer,[c] M. A. Cardoso,[b, d] A. Mayoral,[e] R. A. S. Ferreira,[d] L. D. Carlos,[d] P. Ferreira,[f] P. Almeida,[a] X. Cattoën,[g] M. Wong Chi Man,[h] and V. de Zea Bermudez*[b, i]

Non-porous bridged silsesquioxanes (BSs) were produced by sol-gel reactions and self-directed assembly, in the presence of an acid catalyst and a large excess of water, from bridged organosilane precursors (BOPs) synthesized by click chemistry. The rational design of the compounds, comprising an amine group and alkyl chains with variable length (n), pendant and anchored on a single position to a triazole ring, and the control of acid content (*w*, moles of acid per moles of BOP) enabled the tuning of the morphology and structure of the BSs. At n = 6, 12 and 16, and *w* = 0.2 amorphous hybrids were produced as uniform isotropic micro- to nanospheres. Structuring resulted at n = 16 and *w* = 1.2 or n = 20 and *w* = 0.2, yielding lamellar bilayer structures. In the case of the BS with n = 20 and *w* = 1.2 a lamellar bilayer phase and a minor hexagonal 2D structure emerged. The quite unusual formation of the latter structure was attributed to the presence of a chloride ion close to the proton located between the N(2) atom of the triazole ring and the amine group of the organic spacer, acting as a curvature agent.

Introduction

Materials in biological systems possess a number of features that are not currently found in engineered nanomaterials, including hierarchical structure, organic/inorganic symbiosis, non-equilibrium, self-healing, miniaturization, reconfigurable, and defect-tolerant structures.[1] Materials from the natural world are known to be complex systems[2,3] which provide plenty of inspiring examples of hierarchical arrangement,[3,4] self-similarity growth[5,6] and emergent phenomena. In the last few years biomimetic strategies have been extensively adopted by the community of materials science with the goal of designing innovative materials exhibiting the extraordinary features offered by materials in Nature.

The synthesis of organic/inorganic hybrid materials exhibiting ordered architectures from organosilane precursors represents a very exciting field of research due to their wide range of potential applications.[7,8] The combined use of sol-gel chemistry[9] with self-assembly (SA) processes[10] has been the preferred route to produce them.

The degree of order of the resulting organic/inorganic hybrids systems may be easily tuned by the choice of suitable precursors, which are usually moisture-sensitive organotrialkoxysilanes. The favourite approach for the generation of long-range ordered hybrid mesostructures relies on the molecular design of the organic moiety of the precursor which should include functional groups possessing strong cohesive forces, such as hydrogen bonding (urea-derived systems,[11–16] urethane,[17] π–π,[18,19] polar[20,21] and non-polar van der Waals[14,15,22–25] interactions. A variety of hybrid mesostructures (lamellar, hexagonal and cubic) organized into larger superstructures often displaying different morphologies (fibres, tubes, and helices) have been reported. An entirely different design concept for the production of mesostructured hybrids relies on the use of well-defined oligosiloxane precursors incorporating an alkylsilane core and two or three branched trimethoxysilyl

[a] *Dr. S. C. Nunes, Prof. Dr. P. Almeida*
CICS - Health Sciences Research Center and Chemistry Department
University of Beira Interior
6201-001 Covilhã, Portugal
E-mail: snunes@ubi.pt
[b] *Dr. S. C. Nunes, Dr. M. A. Cardoso, Prof. Dr. V. de Zea Bermudez*
Department Chemistry
University of Trás-os-Montes e Alto Douro
5000-801 Vila Real, Portugal
E-mail: vbermude@utad.pt
[c] *Dr. G. Toquer*
Institut de Chimie Séparative de Marcoule
(UMR 5257 CEA-CNRS-UM2-ENSCM)
BP17171, 30207 Bagnols sur Cèze, France.
[d] *Dr. M. A. Cardoso, Prof. Dr. R. A. S. Ferreira, Prof. Dr. L. D. Carlos*
Department of Physics, CICECO - Aveiro Institute of Materials,
University of Aveiro
3810-193 Aveiro, Portugal.
[e] *Dr. A. Mayoral*
Laboratorio de Microscopias Avanzadas
Instituto de Nanociencia de Aragon
Universidad de Zaragoza
50018 Zaragoza, Spain.
[f] *Dr. P. Ferreira*
Department of Materials and Ceramic Engineering
CICECO - Aveiro Institute of Materials
University of Aveiro
3810-193 Aveiro, Portugal.
[g] *Dr. X. Cattoën*
Inst NEEL
Univ. Grenoble Alpes
Inst NEEL F-38042 Grenoble
F38042 Grenoble, France
[h] *Dr. M. Wong Chi Man*
Institut Charles Gerhardt Montpellier
UMR5253 CNRS-ENSCM-UM
8, rue de l'école normale, 34296 Montpellier, France
[i] *Prof. Dr. V. de Zea Bermudez*
CQ-VR, University of Trás-os-Montes e Alto Douro
5000-801 Vila Real, Portugal

Supporting information for this article is available on the WWW under http://dx.doi.org/10.1002/slct.201601806

groups.[26,27] The organization also depends critically of the judicious selection of experimental parameters[14,15,17,28,29] (e.g., temperature, catalyst, solvent, and precursor concentration) as a means to favour long-range periodicity. Very recently an efficient and original approach was introduced that enabled tuning the structure of aminoundecyltriethoxysilane-derived silsesquioxanes in water in the presence of an acid. The complete proton transfer from the acid to the amine led to the formation of an ammonium headgroup which was responsible for the bending of the interface between the aliphatic chains and the surrounding water. By increasing the size of the acid used as curvature agent, it was possible to tune the organization into bilayers, multibilayer vesicles, cylindral direct micelles or nanofibers.[30,31]

Among the numerous synthetic methods available for the preparation of organotrialkoxysilanes, click chemistry emerges as an especially attractive route.[32,33] This type of methodology, which is characterized by modular reactions that covalently couple molecular building blocks, occurs with high yield and selectivity, under mild and green conditions, using harmless reactants and solvents. The most widely used click reaction is the copper(I)-catalyzed azide-alkyne cycloaddition reaction, termed CuAAC, that has known impressive popularity since its discovery in 2002.[34,35]

Recently, we have introduced a new family of bridged silsesquioxanes (BSs) prepared via classical sol-gel reactions (molar ratio bridged organosilane precursor (BOP)/ethanol/water/tetrahydrofuran (THF) = 1/4/1.5/80) from click chemistry-derived organobridged trialkoxysilane precursors incorporating alkyl chains pendant and anchored on a single position to a triazole ring (Figure 1).[33] The influence of the alkyl chain length

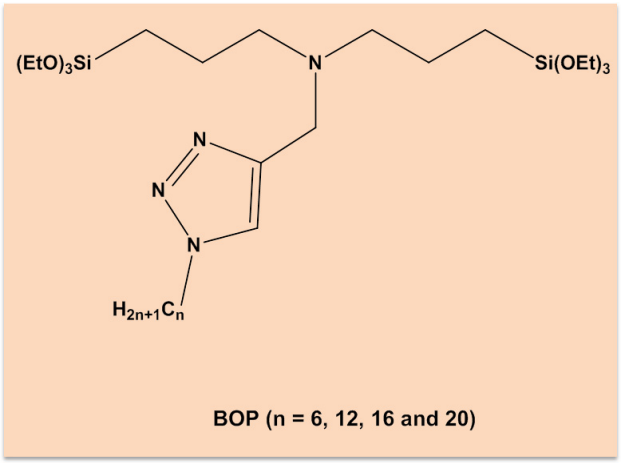

Figure 1. Chemical structure of the BOPs.

on the structuring of these BSs, represented by the notation Cn/siloxane, where n is the number of the carbon atoms of the pendant alkyl chain, was examined for n = 6 and 20. In the case of the material comprising icosanyl chains (C20/siloxane), a hierarchically structured lamellar bilayer organisation displaying a reversible time-independent order/disorder phase transition (onset at 60 °C) was detected. In the essentially amorphous C6/siloxane sample the genesis of a pre-lamellar phase similar to that found in C20/siloxane was identified.

In the present study we have performed the sol-gel synthesis of Cn/siloxane BSs with n = 6, 12, 16 and 20 in the presence a large excess of water (molar ratio of BOP: H_2O:THF = 1:600:70), and upon addition of an acid catalyst (molar ratio BOP: hydrochloric acid (HCl, *w*) = 1:0.2 and 1:1.2). The hydrolytic route performed under acid catalysis has been extensively employed for the production of SA nanostructured BSs incorporating alkyl chains and urea[11] and amide[6,14,15,36] groups.

Results and Discussion

Following our earlier study on the hydrolysis/condensation of Cn/siloxane BOPs in THF medium and in the absence of an external catalyst[33] (the tertiary amine group in the structure acted itself as basic catalyst), we decided to investigate the structure of the materials synthesized at lower pH, by partially or fully neutralizing the basic amine group (0.2 and 1.2 equivalents of HCl, corresponding to pH values of approximately 6 and 2, respectively).

The ^{29}Si MAS NMR spectra of the Cn/siloxane-AC (600:1.2) BS hybrids shown in Figure 2A display resonances between -40 and -80 ppm which are assigned to four types of silicon sites on the basis of the general notation T^x (where x is the number of Si-O–Si bonds): T^0 (CH_2-Si(OR)$_3$), T^1 (CH_2-Si(OSi)(OR)$_2$), T^2 (CH_2-Si(OSi)$_2$(OR) and T^3 (CH_2- Si(OSi)$_3$) (Figure 2 A).[37] The presence of the T^0 site in the case of C16/siloxane (600:1.2) indicates that the polycondensation was not complete in this hybrid (Figure 2A, blue line). Considering that this sample is a bridged system, it is possible that the hydrolysis/condensation reactions might have occurred solely on one of the two trialkoxysilyl groups. This would imply having on one side of the organo-bridged units partially or fully condensed trialkoxy groups (T^1, T^2 and T^3 sites, as manifested in the ^{29}Si MAS NMR spectra) and on the other side remaining unreacted fragments of Si(OEt)$_3$. The dominant signal in the ^{29}Si MAS NMR spectra of C16/siloxane-AC (600:1.2) and C20/siloxane-AC (600:1.2), located at -67 ppm ppm (blue and red thick lines in Figure 2A, respectively), is associated with T^3 environments (Table 1). The fraction of T^x ^{29}Si chemical environments present in each sample, as well as the degree of polycondensation, defined as $c = 1/3\ (T^1 + 2 \times T^2 + 3 \times T^3) \times 100$, are listed in Table 1. The magnitude of c for both Cn/siloxane-AC (600:1.2) BSs with n = 16 and 20 (78 and 77%, respectively, Table 1) suggests the formation of a 2D siliceous network. However, as in the present system cross-links may be established between the two silyl groups of the same molecule, the formation of $SiO_{1.5}$ plates cannot be discarded. The broad resonance centered at −113 ppm in the ^{29}Si MAS NMR spectra of C12/siloxane-AC (600:1.2) (strong, green thick line in Figure 2A) and C6/siloxane-AC (600:1.2) (weak, black thick line in Figure 2A), is assigned to a Q^4 unit (Q^x, Si(OSi)$_x$(OH)$_{4-x}$) (Table 1). The occurrence of this peak suggested that the high acid content promoted the cleavage of the Si-CH_2

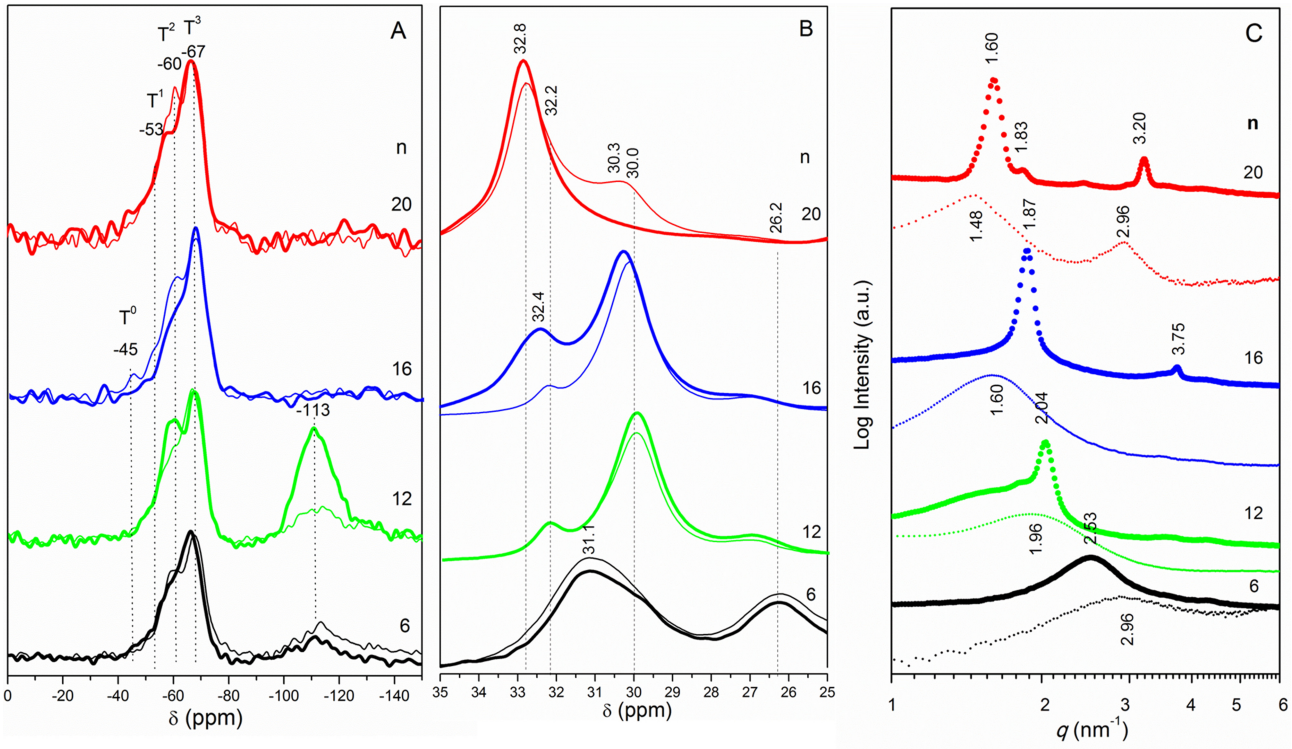

Figure 2. ^{29}Si MAS (A) and ^{13}C CP/MAS (B) NMR spectra, and SAXS profile (C) of the Cn/siloxane-AC (600:*w*) BSs with $w = 0.2$ (thin lines) and $w = 1.2$ (thick lines).

Table 1. ^{29}Si MAS NMR and ^{13}C CP/MAS data (δ in ppm) of the Cn/siloxane-AC (600:*w*) BSs. A and A′ are the fractions of T^x and Q^x chemical environments in %, respectively, and c and d are the polycondensation degrees.

						^{29}Si MAS NMR					
w	n	T^0 (A)	T^1 (A)	T^2 (A)	T^3 (A)	Q^2 (A′)	Q^3 (A′)	Q^4 (A′)	c [*]	D [**]	Empirical Formula
0	20	-	-55.4 (13)	-62.2 (28)	-67.8 (59)	-	-	-	82	-	$R'_{0.5}Si(OR)_{0.5}(O)_{1.2}$
0.2	6	-	-55.0 (11)	-62.1 (22)	-68.1 (47)	-97.0 (3.8)	-105.0 (3.8)	-113.9 (12)	-	82	-
	12	-	-54.0 (3.2)	-58.7 (24)	-67.7 (31)	-96.4 (0.6)	-103.0 (2.9)	-111.4 (38)	-	89	-
	16	-	-57.1 (13)	-62.1 (24)	-68.1 (62)	-	-	-	83	-	$R'_{0.5}Si(OR)_{0.5}(O)_{0.8}$
	20	-	-58.0 (28)	-62.1 (33)	-68.9 (39)	-	-	-	72	-	$R'_{0.5}Si(OR)_{0.9}(O)_{1.0}$
1.2	6	-	-57.1 (11)	-60.6 (25)	-66.9 (48)	-95.0 (0.7)	-102.0 (3.0)	-112.6 (12)	-	83	-
	12	-	-53.8 (14)	-59.2 (22)	-67.2 (50)	-90.0 (0.5)	-106.3 (7.5)	-114.5 (6.5)	-	81	-
	16	-45.8 (2.7)	-53.9 (12)	-59.9 (33)	-67.1(52)	-	-	-	78		$R'_{0.5}Si(OR)_{0.3}(O)_{1.2}$
	20	-	-55.8 (22)	-60.7 (24)	-66.7(53)	-	-	-	77		$R'_{0.5}Si(OR)_{0.3}(O)_{1.1}$

					^{13}C CP/MAS NMR					
n	6	12			16			20		Attribution
w	0.2	1.2	0.2	1.2	0.2	1.2	0	0.2	1.2	
	144.9	-	143.0	-	145.0	-	145.1	144.0		***C*quaternary**$_{triazole}$
	137.6	137.2	-	137.1	-	137.1	-	-	137.1	***C*quaternary**$_{protonated\ triazole}$
	123.9	128.6	125.0	128.2	125.0	127.9	123.1	125.0	127.7	***CH***$_{triazole}$
	56.3	55.2	55.4	55.2	56.8	55.6	56.4	56.8	55.2	$(\mathbf{C}H_2)_2NCH_2/SiO\mathbf{C}H_2CH_3$
	50.2	50.8	50.4	50.6	50.3	50.8	50.1	50.3	50.9	$CH_2\mathbf{C}H_2$-$N_{triazole}$
	31.2	31.1	32.3	32.1	32.1	32.4	-	33.0	32.8	$\mathbf{C}H_2$ (alkyl chains) all trans
	-	-	30.0	29.9	30.2	30.2	30.1	30.2	-	$\mathbf{C}H_2$ (alkyl chains) *gauche*
	26.3	26.3	27.2	27.1	27.0	27.1	27.0	26.8	28.9	$\mathbf{C}H_2$ (alkyl chains)
	22.5	22.5	22.9	22.8	23.0/21.0	22.9	23.0	23.0/21.0	24.5	$SiCH_2\mathbf{C}H_2$ / $CH_2\mathbf{C}H_2CH_3$
	-	18.7	20.6	18.9	-	18.9	-	-	18.8	$OCH_2\mathbf{C}H_3$
	14.0	14.11	14.2	14.11	14.2	14.4	14	14.2	14.5	$CH_2CH_2\mathbf{C}H_3$
	10.9	9.98	10.7	10.3	10.9	10.0	11.0	10.9	10.2	$Si\mathbf{C}H_2CH_2$

[*] $c = {}^1/_3 \times (1 \times \%T^1 + 2 \times \%T^2 + 3 \times \%T^3)$ [**] $d = {}^1/_3 \times (1 \times \%T^1 + 2 \times \%T^2 + 3 \times \%T^3) + 1/4\ (1x \times \%Q^1 + 2 \times \%Q^2 + 3 \times \%Q^3 + 4 \times Q^4)$.

bond in the BSs containing short alkyl chains (n $\leq$ 12). However, the analysis of the ^{29}Si MAS NMR spectra of the Cn/siloxane-AC (600:0.2) BSs with n = 6 and 12 (Figure 2A, black and green thin lines, respectively) and C20/siloxane (600:0) (Figure S1 of Supplementary Information) demonstrates that the characteristic Q^4 resonances persisted. Thus, we are led to conclude that the BOPs precursors with short alkyl chains (n $\leq$ 12) are quite unstable in the presence of large amounts of water. However, no precise explanation can be given for this partial Si–C bond cleavage, which has only been scarcely reported in the literature[38–40].

The ^{13}C CP/MAS NMR spectra of the Cn/siloxane-AC (600:0.2) and Cn/siloxane-AC (600:1.2) BS materials are reproduced in Figure S2 of Supplementary Information. The position (δ) and assignment of the resonance peaks are given in Table 1. These spectra display signals originating from the carbon atoms of the Si- bonded propyl chains, of the triazole rings and of the pendant alkyl chains anchored on the rings, which confirm the integrity of the organic functional groups of the BOPs. They also demonstrate that the hydrolysis reaction did not go to completion in the case of the Cn/siloxane-AC (600:1.2) samples, as indicated by the presence of the peaks around 58 and 18 ppm, associated with the resonance of ethoxyl carbon atoms. The existence of a resonance at 10 ppm confirms that only a small percentage of the Si-CH_2 bonds were cleaved during the reaction (Figure S2 of Supplementary Information and Table 1). It is noteworthy that the chemical shift of the triazole quaternary carbon moved from *ca.* 145 ppm for the Cn/siloxane-AC (600:*w*) materials with *w* = 0 and 0.2, the typical resonance for neutral triazole rings, to 137 ppm in the case of *w* = 1.2 (Table 1). A simple calculation of ^{13}C NMR chemical shifts using ChemDraw software suggests that the triazole rings were either protonated on the N(2) nitrogen atom, or were at least strongly hydrogen-bonded between the amine group and the triazole ring. In addition, the ^{13}C CP/MAS NMR data provided valuable information on the degree of conformational order of the pendant alkyl chains of the BS samples. The presence of a dominant peak in the ^{13}C CP/MAS NMR spectra of C6/siloxane-AC (600:*w*) (black thin and thick lines in Figure 2B) at 31.1 ppm, of C12/siloxane-AC (600:*w*) (green thin and thick lines in Figure 2B) at 30.0 ppm, and of C16/siloxane-AC (600:0.2) (blue thin line in Figure 2B) at 30.3 ppm and the existence of a less intense peak in the ^{13}C CP/MAS NMR spectra of C12/siloxane-AC (600:*w*) (green thin and thick lines in Figure 2B) and C16/siloxane-AC (600:0.2) (blue thin line in Figure 2B) at 32.2 ppm (green thin and thick lines in Figure 2B) and of C16/siloxane-AC (600:1.2) (blue thick line in Figure 1B) at 32.4 ppm point out that the great majority of the pendant alkyl chains in these samples adopted *gauche* conformations, with a minor proportion of all-*trans* conformations in the C12/siloxane-AC (600:*w*) and C16/siloxane-AC (600:0.2) samples and a more significant content in the case of C16/siloxane-AC (600:1.2).[41–43] The unusually low δ value of the peak produced at 26.2 ppm by the C6/siloxane-AC (600:*w*) BSs with *w* = 0.2 and 1.2 (black thin and thick lines in Figure 2B) is worth mentioning. We note that Earl and Van der Hart[44] found a peak at 27.84 $\pm$ 0.10 ppm in the ^{13}C CP/MAS NMR spectrum of neat cyclohexane (C_6H_{12}), a compound which is constrained in all-*gauche* conformations (g + g-). In the ^{13}C CP/MAS NMR spectrum of C20/siloxane-AC (600:1.2) a single prominent resonance is found at 32.8 ppm (red thick line in Figure 2B), pointing out that in this material all the pendant alkyl chains virtually adopted zig-zag ordered conformations.[41–43] This δ value is not too different from that reported for the crystalline component of high molecular weight linear polyethylene (34.36 $\pm$ 0.55 ppm), in which the alkyl chains adopt ideally only all-*trans* conformations.[44] In the case of C20/siloxane-AC (600:0.2), although the 32.8 ppm peak dominates, another one, less strong, is distinguished at ca. 30.3 ppm (red thin line in Figure 2B). These data clearly demonstrate that a higher acid content did not affect the relative ratio of all-*trans*/*gauche* conformers in the hybrids with n = 6 and 12 (thick black and green lines in Figure 2B, respectively), but that, in contrast, it had a dramatic impact in the case of the BSs with longer pendant chains (n > 12).

The SAXS profiles and the XRD patterns of the Cn/siloxane-AC (600:*w*) BSs with *w* = 0.2 (thin lines) and *w* = 1.2 (thick lines) in the 1–6 nm^{-1} and 10–20 nm^{-1} *q* ranges (where $q = 4\pi\sin\theta/\lambda$ where 2θ is the scattering angle and λ is the wavelength) are represented in Figure 2C and Figure S3 of Supplementary Information, respectively. Close analysis of the profile of the XRD and SAXS patterns shows that the length of the alkyl chains and the acid content influenced significantly the nanostructure of the BS hybrids.

In the low-*q* range ($q < 6$ nm^{-1}) the SAXS profiles of the Cn/siloxane-AC (600:0.2) BSs with n = 6, 12 and 16 exhibit a single broad weak peak centred at 2.96, 1.96 and 1.60 nm^{-1}, respectively (thin black, green and blue lines in Figure 2C, respectively), assigned to scattering interference between siliceous regions separated by the organic moieties (i.e., triazole rings carrying the pendant alkyl chains) and corresponding to average inter-region distances of 2.1, 3.2 and 3.9 nm, respectively.[45–47] All these materials are mostly amorphous judging from the breadth of the peaks. In contrast, extending the alkyl chain length to n = 20, or increasing the acid content for n = 16 or 20 from *w* = 0.2 to 1.2 led to a structuring of the materials. In fact, C16/siloxane-AC (600:1.2) gave rise to a pair of peaks at 1.87 and 3.75 nm^{-1} (thick blue line in Figure 2C) and C20/siloxane-AC (600:0.2) produced two peaks at 1.48 and 2.96 nm^{-1} (red thin line in Figure 2C). The first peak produced by both materials represents the 1st of the y^{th} order peaks of lamellar bilayer structures with spacings *l* = 3.4 and 4.2 nm (where $l = 2\pi/q$), respectively (Scheme 1). The increase of the interlamellar distance observed (0.8 nm) may be correlated with a combination of two effects: (1) The presence of four additional carbon atoms in the pendant alkyl chain, which theoretically implies an increase of 0.52 nm/alkyl chain in an ordered conformation (assuming an average C–C distance of 0.13 nm); (2) The higher degree of conformational order of the alkyl chains in C20/siloxane-AC (600:0.2). Indeed, according to the ^{13}C CP/MAS NMR data, in C20/siloxane-AC (600:0.2) most of the alkyl chains were fully extended and highly ordered (essentially all-*trans* conformations), whereas in C16/siloxane-AC (600:1.2) the great majority of the alkyl chains were highly

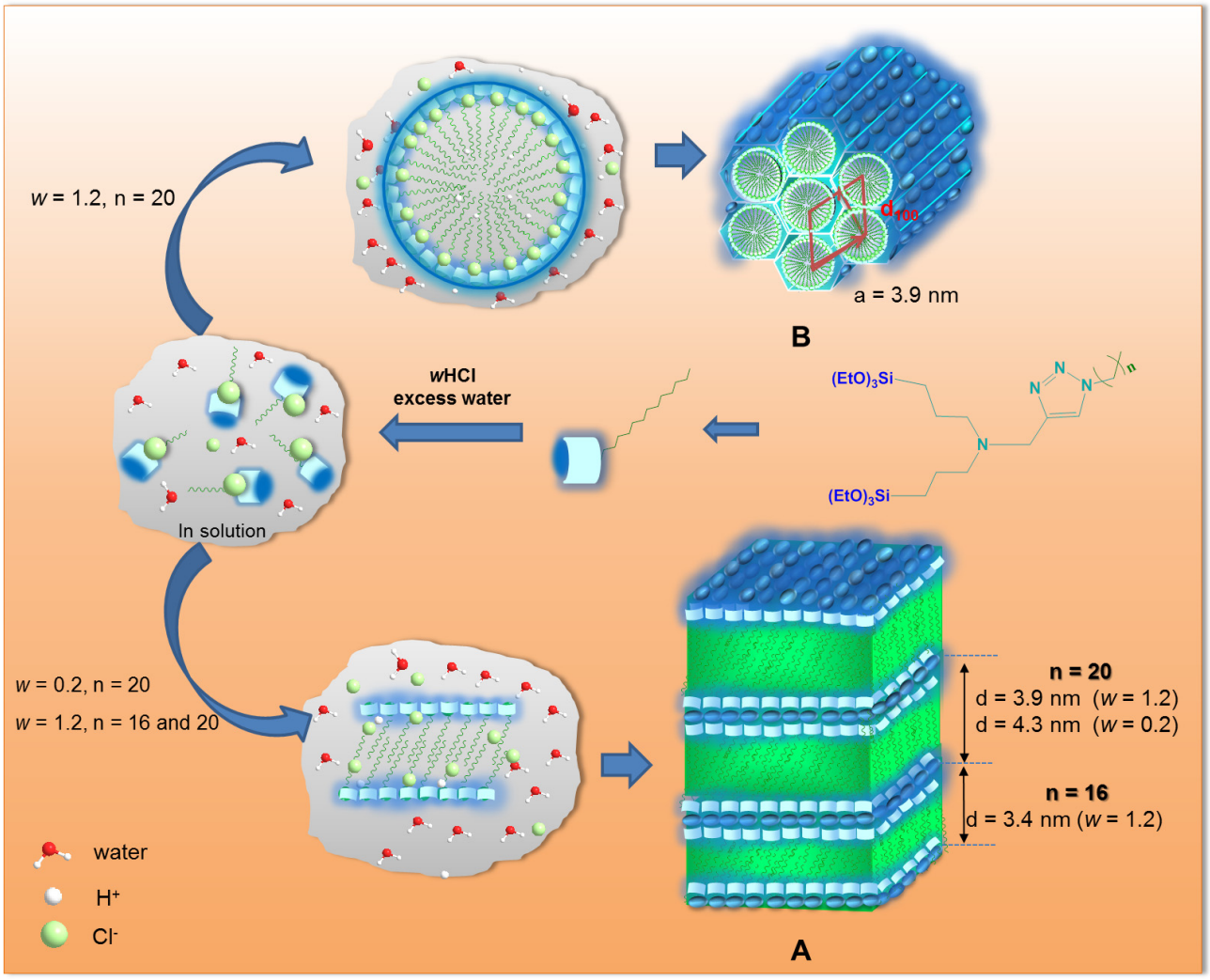

Scheme 1. Schematic representation of the lamellar structures (**A**) of the C16/siloxane-AC (600:1.2) and C20/siloxane-AC (600:0.2) BSs and of the hexagonal structure (**B**) of the C16/siloxane-AC (600:1.2) BS, depending on the acid content and the length of the pending alkyl chain.

disordered (essentially all-*gauche* conformations). Structurally the C20/siloxane-AC (600:1.2) sample is completely different from the above mentioned samples but by far the most interesting of the whole series. Its SAXS profile exhibits in the low-q range a complex profile composed of a prominent peak a 1.60 nm^{-1}, a shoulder at 1.83 nm^{-1} and a strong peak at 3.20 nm^{-1} (thick red line in Figure 2C). The peaks at 1.60 and 3.20 nm^{-1} were assigned to a lamellar structure **A** with inter-lamellar distance $l = 3.9$ nm, whereas those located at 1.83 and 3.20 nm^{-1} were associated with the first two peaks ((100) and (110) reflections, respectively) of a minor hexagonal structure **B** with lattice parameter $a = 3.9$ nm (where $a = 2d_{100}/\sqrt{(3)}$ and $d_{100} = 3.43$ nm). It is noteworthy that the lattice parameters of **A** and **B** (i.e., l and a, respectively) are identical, which is not surprising, as both distances correspond roughly to the length of two partially interdigitated alkylsiloxanes (Scheme 1). To date 2D hexagonal structures have been scarcely reported for alkylsilsesquioxanes.[30,33] They were mainly observed when the size of the polar head formed by hydrolysis of the alkoxysilane group was increased. In the case of C20/siloxane-AC (600:1.2), two effects exerted a major influence: (1) The size of the alkyl chain was long enough to allow for strong hydrophobic interactions promoting the structuring of the material; (2) The protonation of the amine-triazole fragment by HCl enabled the increase of the volume of the polar head.[30,33] In contrast, when only 20% of the precursor molecule were protonated (C20/siloxane-AC (600:0.2)), the hexagonal order did not emerge. The slight decrease of the interlamellar spacing between the major phase **A** (lamellar) of C20/siloxane-AC (600:0.2) and that of C20/siloxane-AC (600:1.2) (from 4.3 to 3.9 nm) is counterintuitive, considering that practically all the alkyl chains were fully extended in the latter hybrid. However, it is important to remind that there was an important difference in the reaction conditions of the two syntheses in terms of pH. Indeed, while at pH $\approx$ 2 (1.2 equivalents of HCl) the hydrolysis was very fast and the condensation rate was low, under slightly acidic conditions (pH $\approx$ 6, 0.2 equivalents of HCl), the condensation was much faster. We have already shown that the structuring

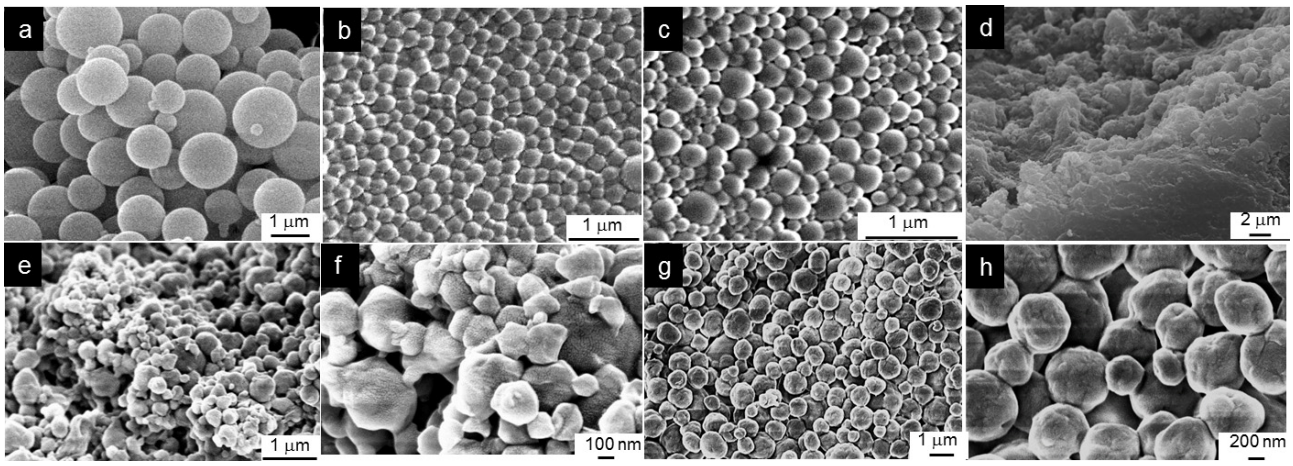

Figure 3. SEM images of the Cn/siloxane-AC (600:0.2) BSs (top) with n = 6 (a), 12 (b), 16 (c) and 20 (d) and of the Cn/siloxane-AC (600:1.2) BSs (bottom) with n = 16 (e and f) and 20 (g and h).

of BSs was possible over long ranges at pH ≈ 2.[14,48,49] At this pH the hydrolyzed species have time to form and subsequently self-assemble before the condensation takes place to cross-link the assembled entities.[49,50] In the present case, we may infer that the degree of interdigitation of the alkyl chains was higher at pH ≈ 2, leading to a decrease of the interlamellar distance.

In the high-q region ($q > 5\ nm^{-1}$) the XRD patterns of the Cn/siloxane-AC (600:0.2) BSs with n = 6, 12 and 16 exhibit a broad, non-resolved band, Gaussian in shape, at ca. $14.0\ nm^{-1}$ (Figure S3 of Supplementary Information). In the case of C20/siloxane-AC (600:0.2), C16/siloxane-AC (600:1.2) and C20/siloxane-AC (600:1.2) the band is considerably narrower and its intensity maximum was shifted to $15.1\ nm^{-1}$ (Figure S3 of Supplementary Information). Globally both effects suggest that the longer pendant chains and a higher acid content promoted a higher degree of structural order in the latter three samples. Whenever the high-q region of BSs is partially or completely resolved, rich structural information may be retrieved. For instance, in the case of di-amidosil BSs[54] distinct peaks were found at: (1) $14.2\ nm^{-1}$, ascribed to amide-amide spacings ($d_{AA} = 0.44$ nm);[17] (2) $14.7\ nm^{-1}$, attributed to ordering within the 2D siloxane domains ($d_{SiOSi} = 0.43$ nm)[45] (3) 15.1 and $15.6\ nm^{-1}$ (shoulder, $d_{CCg} = 0.41$ and 0.40 nm, respectively), associated with alkyl chains in *gauche* conformations; (4) 16.8, 18.2, 19.2 and 20.8. nm^{-1} ($d_{CCt} = 0.37$, 0.34, 0.32 and 0.30 nm respectively), attributed to alkyl chains in all-*trans* conformations.[17,52,53] Unfortunately, in the present case the high-q region is not resolved and consequently the assignment is subject to much uncertainty. However, it is possible to state that the band profile is clearly the result of the convolution of two main contributions originating from ordering within the 2D siloxane domains and from the type of alkyl chains conformers present. The upshift of the intensity maximum observed in the case of C20/siloxane-AC (600:0.2), C16/siloxane-AC (600:1.2) and C20/siloxane-AC (600:1.2) is consistent with the considerably higher proportion of all-*trans* conformers existent in these three samples, as pointed out by ^{13}C CP/MAS NMR data.

The SEM images of Cn/siloxane-AC with n = 6, 12 and 16 (Figures 3a, 3b and 3c, respectively) demonstrate that these hybrids are produced as uniform isotropic micro- to nano-spheres of increasing degree of packing. In contrast, the SEM image of C20/siloxane-AC (600:0.2) (Figure 3d) showed micrometric plates of nanometer thickness, corroborating the SAXS data. In the case of C16/siloxane-AC (600:1.2), no evidences of a lamellar structure were found in the SEM images (Figures 3e and 3f) which show irregular micro- to nano-sized objects with quasi-spheroidal to hexagonal shapes. The latter facetted hexagonal particles are similar to those formed in C20/siloxane-AC (600:1.2) (Figures 3g and 3h). The heterogeneous aspect of C16/siloxane-AC (600:1.2) on the SEM micrographs is consistent with the broader peaks observed in the SAXS profile of Figure 3C (thick blue line), giving additional support to the possible presence of hexagonal structures. In the TEM images of C16/siloxane-AC (600:1.2) (Figures 4Aa and 4Ab) areas with reduced order and others exhibiting parallel patterns with an average spacing of 2.43 nm are visible. This spacing is of the same order of magnitude as the interlamellar distance retrieved from SAXS ($l = 3.40$ nm). For C20/siloxane-AC (600:1.2) the SEM data provided evidence of the formation of highly packed nanometer-size facetted objects with essentially hexagonal morphology (Figures 3g and 3h). Only parallel patterns were observed, however, by TEM (Figure 4 Ba-d). The 3.5 nm spacing observed is of the same order of magnitude of the d_{100} and a spacings (3.9 nm) derived from SAXS data for the lamellar and hexagonal phases, respectively (Figure 4 Ba-d). In the TEM images of the C16/siloxane-AC (600:1.2) sample a few completely round-shape particles were also detected (Figure S4 of Supplementary Information). These amorphous particles resemble those observed by SEM in the Cn/siloxane-AC (600:0.2) BSs with n = 6, 12 and 16 (Figure 3a, 3b and 3c, respectively), corroborating the disordered nature of these materials, as indicated by SAXS (thin black, green and blue lines of Figure 3C, respectively). Figure S4 of Supplementary Information displays the TEM image of a 200 nm particle, where no

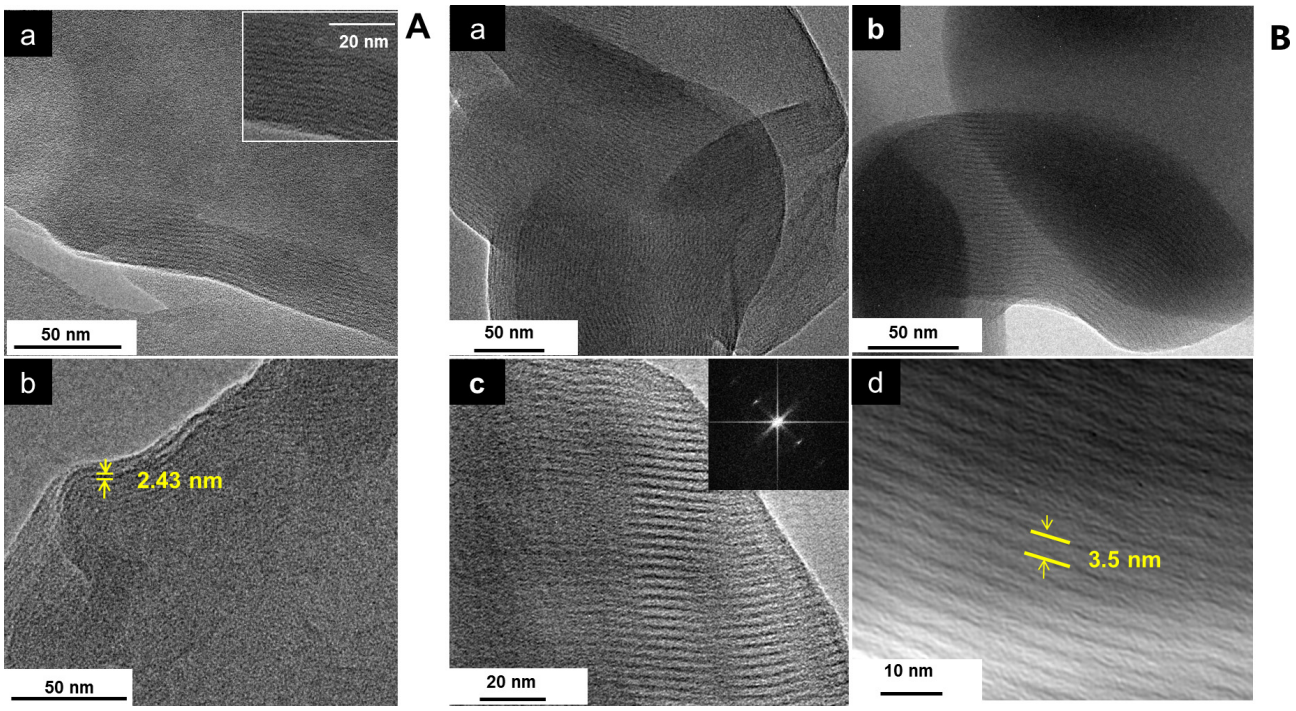

Figure 4. TEM images of the C16/siloxane-AC (600:1.2) (A) and C20/siloxane-AC (600:1.2) (B) BSs.

ordered structure could be identified. At last, it is worth mentioning that the N_2 adsorption/desorption isotherms of Cn/siloxane-AC (600:1.2) with n = 16 and 20 provided evidence of the non-porous nature of both samples (Figure S5 of Supplementary Information).

It is of interest to analyse at this point the DSC data, because this technique provides rich information about the thermodynamic behaviour of polymer chains[14,15,33,54,55]. The DSC curves of the Cn/siloxane-AC BS (600:*w*) BSs with $w = 0.2$ and 1.2 in the 20–200 °C range are represented in Figure 5 (thin and thick lines, respectively). The thermograms of the Cn/siloxane-AC (600:0.2) BSs with n = 6, 12 and 16 (black, green and blue thin lines of Figure 5) confirm the amorphous nature of these BS hybrids. The DSC curve of C16/siloxane-AC (600:1.2) exhibits a weak endotherm centred at about 33 °C (thick blue line of Figure 5). In the case of C20/siloxane-AC (600:0.2) the DSC curve displays two endothermic events centred at 48 and 67 °C, whereas C20/siloxane-AC (600:1.2) gave rise to an endotherm (shoulder) at 56 °C, of unknown origin, and to two sharp endothermic peaks at 68 and 73 °C (very strong). We tentatively ascribe the pair of endotherms at 68 and 73 °C in the DSC curve of C20/siloxane-AC (600:1.2) with the lamellar phase **A** and the hexagonal phase **B.** Considering that the latter structure exists in a minor proportion in this sample, we feel tempted to associate phase **B** with the 68 °C peak. Furthermore, as the latter thermal event is also produced by C20/siloxane-AC (600:0.2), we are led to suppose that phase **B** also probably exists in this BS, in a minor proportion. Evidences of the occurrence of this phase in the SAXS profile of the C20/siloxane-AC (600:0.2) could not be found, however, because of

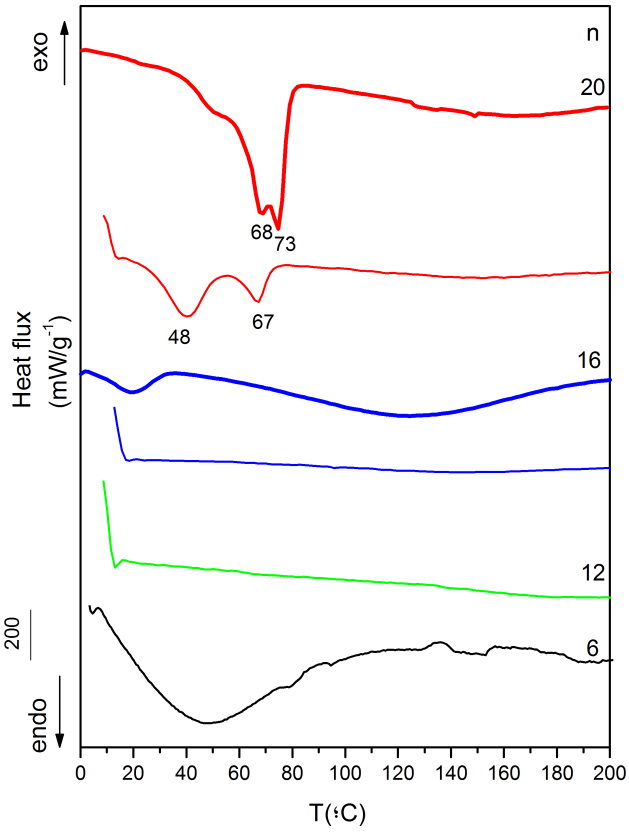

Figure 5. DSC curves of the Cn/siloxane-AC (600:*w*) BSs with $w = 0.2$ (thin lines) and $w = 1.2$ (thick lines).

the broadness of the peaks centred at 1.48 and 2.96 nm^{-1} (thin red line in Figure 3C) due to the main lamellar structure. In addition we ascribe the endotherms produced by C16/siloxane-AC (600:1.2) and C20/siloxane-AC (600:0.2) at 33 and 48 °C, respectively, with the order/disorder phase transition of the pendant alkyl chains of the lamellar bilayer structures formed in these two samples. We recall that in the former sample, unlike in the latter, the proportion of all-*trans* conformations is far from being dominant, as indicated by ^{13}C CP/MAS NMR. This fact could account for the lower temperature value of this thermal event.The ATR-FTIR spectra of the Cn/siloxane-AC BSs in the ν_sCH_2 and ν_aCH_2 regions are reproduced in Figure 6A. The inspection of the ν_sCH_2 and ν_aCH_2 bands is useful, because their frequency, width and height are sensitive to the *gauche/trans* conformer ratio and to the intermolecular interactions between the alkyl chains. The ATR-FTIR spectrum of C6/siloxane-AC (600:0.2) in the ν_aCH_2 and ν_sCH_2 region displays two broad bands at 2928 and 2861 cm^{-1} (thin black line of Figure 6A and Table S2 of Supplementary Information), an indication that the alkyl chains adopted *gauche* conformations and were therefore disordered. This result is in perfect agreement with the XRD, ^{13}C CP/MAS NMR and DSC data. The ν_aCH_2 and the ν_sCH_2 ATR-FTIR bands of the other Cn/siloxane-AC (600:*w*) BSs are shifted to lower frequencies. In the case of C12/siloxane-AC (600:0.2) (thin green line of Figure 6A and Table S2 of Supplementary Information) and C16/siloxane-AC (600:*w*) (blue lines of Figure 6A and Table S2 of Supplementary Information) these features are located at 2921 and around 2851 cm^{-1} in the ATR-FTIR spectra, meaning that the ordered (all-*trans* conformations) and disordered (*gauche* conformations) alkyl chains coexisted in both materials. The ATR-FTIR spectra of the C20/siloxane-AC (600:*w*) BSs with $w = 0.2$ (thin red line of Figure 6A) and 1.2 (thick red line of Figure 6A) display two intense features at 2917/2916 cm^{-1} (fwhm = 23/16 cm^{-1}) and around 2849/2849 cm^{-1} (full-width-at-half-maximum (fwhm) = 15/10 cm^{-1}) (Figure 6A and Table S2 of Supplementary Information), pointing out that the pendant alkyl chains adopted essentially all-*trans* conformations. However, the considerably lower band fwhm values produced by C20/siloxane-AC (600:1.2) with respect to those of C20/siloxane-AC (600:0.2) support that practically all the alkyl chains in the former hybrid present material were fully stretched, highly packed and therefore entirely crystalline,[56–60] a result that corroborates the ^{13}C CP/MAS NMR data.

The νCH_2 region of the FT-Raman spectrum of C16/siloxane-AC BS (600:1.2) exhibits bands at 2890 and 2851 cm^{-1} and a shoulder at 2930 cm^{-1} (thick blue line of Figure 6B and Table S2 of Supplementary Information). The events at 2890 and 2851 cm^{-1} are attributed to ν_aCH_2 and ν_sCH_2 modes, respectively, and the event at 2930 cm^{-1} is ascribed to the Fermi resonance between the ν_sCH_2 fundamental with the many overtones of the δCH_2 vibrations. The frequency and fwhm of ν_aCH_2 and ν_sCH_2 modes are characteristic of alkyl chains in the amorphous state (*gauche* conformations). In the FT-Raman spectrum of C20/siloxane-AC BS (600:1.2) the νCH_2 region displays two intense events at 2880 and 2846 cm^{-1}, indicating a significant increase of the proportion of all-*trans* conformers.[61,62] This finding is in perfect agreement with the above data.

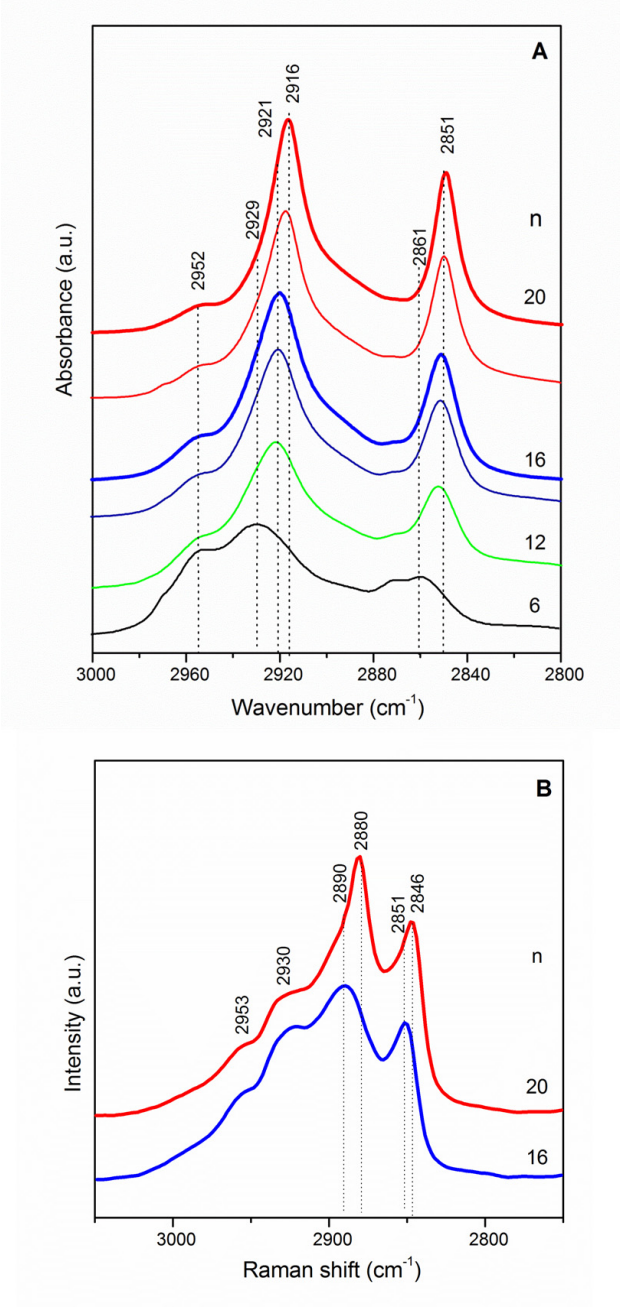

Figure 6. ATR-FTIR spectra of the Cn/siloxane-AC (600:*w*) BSs with x = 0.2 (thin lines) and *w* = 1.2 (thick lines) (A) and FT-Raman spectra of selected Cn/siloxane-AC (600:1.2) BSs (B) in the ν_aCH_2 and ν_sCH_2 regions..

The birefringence of C20/siloxane-AC (600:1.2) detected in the POM image recorded between crossed polarizers (Figure 7) indicates submicrometric anisotropy. The contact angle calculated for this sample (Inset of Figure 7) was 109.6 ± 1.6 °, indicating that the hybrid is hydrophobic.

It was of interest to examine the photoluminescence features of the two ordered samples C16/siloxane-AC (600:1.2) and C20/siloxane-AC (600:1.2). Under UV/visible excitation both

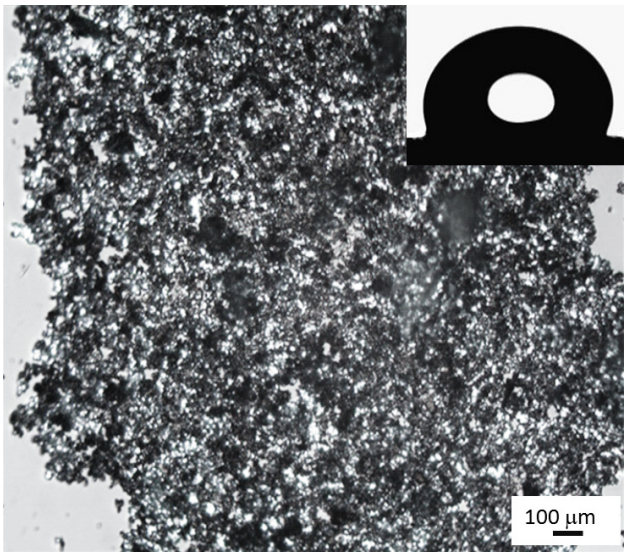

Figure 7. POM (crossed polarizers) image of C20/siloxane-AC (600:1.2) (Scale 100 µm). Inset: picture of water droplet on its surface.

BSs displayed a broad emission band (fwhm, 5000 cm^{-1}) in the visible spectral region (Figure 8). We note that the broad band is formed of, at least, two components peaking at ≈422 and ≈480 nm, as clearly evidenced for C16/siloxane-AC (600:1.2) (Figure 8b). The presence of more than one emission component was also demonstrated by monitoring the excitation spectra along the emission band (Figures 8c and 8d). At lower monitoring wavelength (< 430 nm), the excitation spectra was dominated by a component at ≈355-360 nm also revealing a low-relative intensity one at ≈270 nm. As the wavelength monitoring increased the spectra peak position deviated toward the red and there was an increase in the relative intensity of the component at 270 nm. The low- and high-wavelength components observed might be associated with the preferentially excitation of the siliceous- and amine-related components, as reported for similar hybrid materials.[63–65]

The absolute emission quantum yield of C20/siloxane-AC (600:1.2) and C16/siloxane-AC (600:1.2) BSs, both synthesized in the presence of an acid catalyst, were measured under the two excitation wavelengths at 270 and 360 nm, being, however, below the detection limits of our experimental apparatus (0.01). This result can be tentatively explained on the basis of an in-depth investigation of the amidosils carried out by our group. We first showed that the addition of an acid catalyst significantly enhanced the emission quantum yield of mono-amidosils[15] More recently we demonstrated for the first time that the degree of order of the amide-amide hydrogen-bonded network primarily dictated the magnitude of the emission quantum yield of mono- and di-amidosils, regardless of the degree of order of the material itself.[36] Therefore, in the present case the very low absolute emission quantum yield values (<0.01) of the ordered C16/siloxane-AC (600:1.2) and C20/siloxane-AC (600:1.2) BSs may be interpreted as an indication that the proton recombinations taking place between the triazole N(2) atoms and the amine moieties, as indicated by ^{13}C CP/MAS NMR data, presumably quenched the photoluminescence.

In this study the critical role played by the design of a BOP on the properties of the final BSs has been demonstrated. The chemical structure of the new BOP prepared via click chemistry, including an amine group and incorporating alkyl chains with variable length, pendant and anchored on a single position to a triazole ring, and the addition of an acid catalyst allowed us to confirm that, similarly to what has been reported for other BS systems, the inclusion of longer alkyl chains and a high HCl concentration (pH ≈ 2) favored the formation of lamellar bilayer and ultimately hexagonal 2D phases. Moreover were found evidences that the unusual emergence of the latter structure was linked to the presence of a chloride ion (Cl^-) next to the proton located between the N(2) atom of the triazole ring and to the amine group of the organic spacer. In practice, this anion increased the volume around these two moieties, acting as an efficient curvature agent.[30]

Conclusions

Herein, we introduced a new simple approach to synthesize, by the sol-gel process and self-directed assembly, BSs with variable structure (from amorphous to lamellar bilayer or ultimately hexagonal 2D) from novel BOPs, obtained by click chemistry, incorporating alkyl chains with different length (C_n, with n = 6, 12, 16 and 20) pendant and anchored on a single position to a triazole ring. These precursor molecules, which were hydrolyzed in a large excess of water and in the presence of HCl either in neutral or acidic medium, yielded BSs noted as C_n/siloxane-AC (600:*w*), where AC stands for acid catalysis, and 600 and *w* = 0.2 and 1.2 represent the moles of H_2O and HCl, respectively, per mole of BOP. The Cn/siloxane-based BSs with short alkyl chains (n ≤ 12) were slightly unstable under the reaction conditions employed. Structuring was only achieved with BOPs with longer alkyl chains (n ≥ 16) and higher acid content (*w* = 1.2). The BSs with n = 6, 12 and 16 and *w* = 0.2 were produced as uniform isotropic micro- to nanospheres of increasing degree of packing. In contrast, the C20/siloxane-AC (600:0.2) BS exhibited a lamellar structure with an interlamellar distance *l* of 4.2 nm and was produced as micrometric plates of nanometer thickness. In the case of the C16/siloxane-AC (600:1.2) sample, synthesized with higher acid content, we also detected the formation of a lamellar structure (*l* = 3.4 nm). This material was obtained as irregular sized micro- to nano-objects with quasi-spheroidal to hexagonal shapes. In C20/siloxane-AC (600:1.2), containing the longest chains and the highest acid concentration, highly packed nanometer-size objects with essentially lamellar bilayer morphlogy with a minor hexagonal 2D structure. The presence of Cl^- ions close to the siliceous region of the hybrid material may account for a higher curvature of the transient amphiphiles formed, giving rise to this structure scarcely encountered for organosilicas. Future work will focus on the structural consequences arising from the use of acids including different anions belonging, for instance, to the carboxylate series.[30]

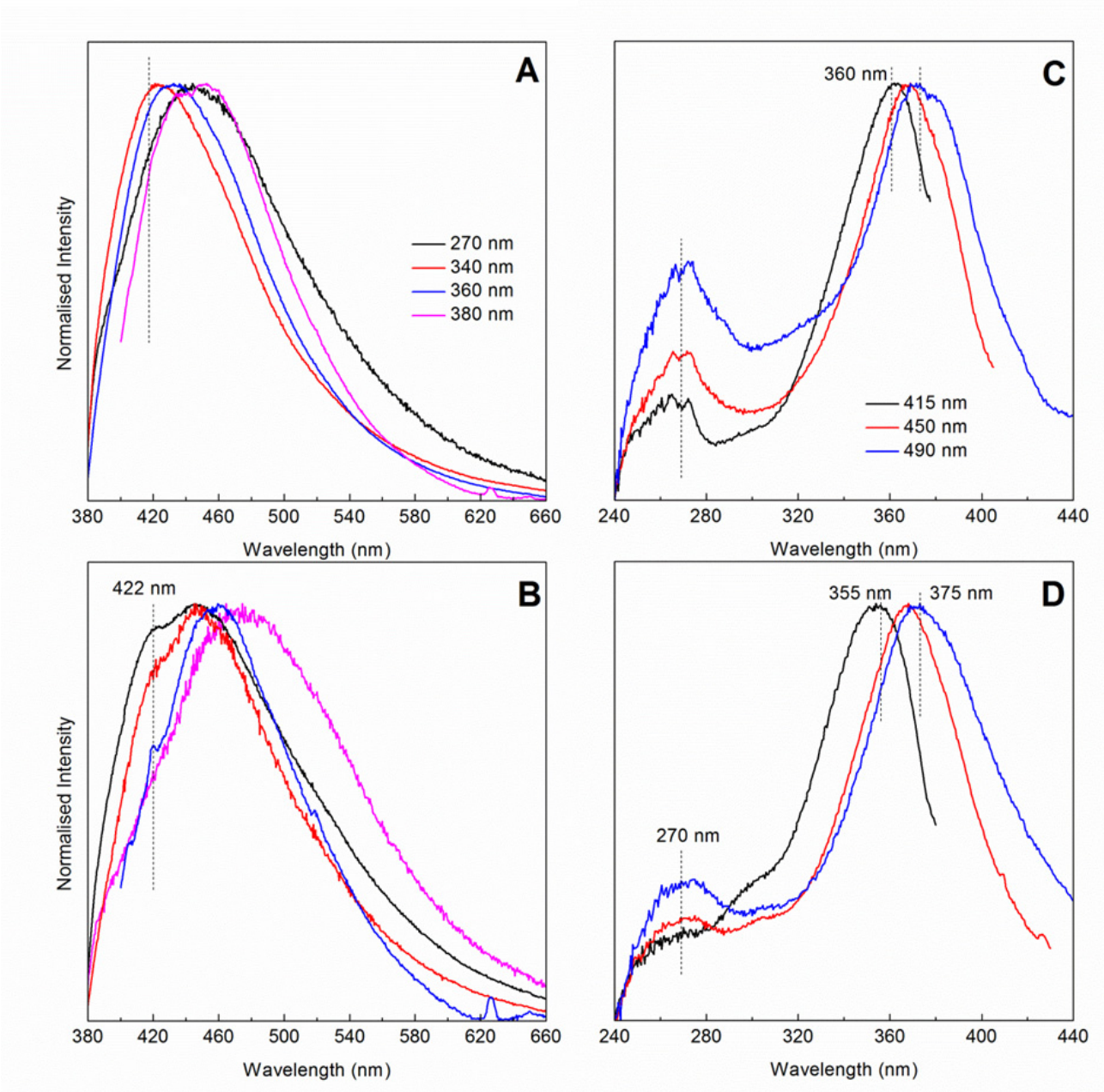

Figure 8. Room-temperature emission (left) and excitation (right) spectra of the C20/siloxane-AC (600:1.2) (a and c) and C16/siloxane-AC (600:1.2) (b and d) BSs. The excitation and monitoring wavelengths are indicated in (a) and (c), respectively.

Acknowledgements

This work was supported by FEDER (POCI-01-0145-FEDER-016884, POCI-01-0145-FEDER-007491 and POCI-01-0145-FEDER-007679) and Fundação para a Ciência e a Tecnologia (FCT) (contracts PTDC/CTM-NAN/0956/2014, UID/QUI/00616/2013, UID/Multi /00709/2013 and UID/CTM/50011/2013 CICECO-Aveiro Institute of Materials). S. C. Nunes and P. Ferreira acknowledge FCT for the grants (SFRH/BPD/63152/2009 and IF/00327/2013, respectively). The authors thank Dr. Sónia Sousa and Prof. Ana Ramos (University of Beira Interior) for the contact angle measurements.

Conflict of Interest

The authors declare no conflict of interest.

Keywords: acid-catalyst · bridged silsesquioxanes · click chemistry · nanostructures · sol-gel process

[1] B. Bhushan, *Phil. Trans. R. Soc. A.* **2009**, *367*, 1445–1486.
[2] P. W. Anderson, *Science* **1992**, *177*, 393–396.
[3] N. Goldenfeld, L. P. Kadanoff, *Science* **1999**, *284*, 87–90.
[4] S. Nikolov, M. Petrov, L. Lymperakis, M. Friák, C. Sachs, H.-O. Fabritius, D. Raabe, J. Neugebauer, *Adv. Mater.* **2010**, *22*, 519–526.

[5] B. Mendelbrot. *Science* **1967**, *156*, 636–638.
[6] S. C. Nunes, C. B. Ferreira, R. A. S. Ferreira, L. D. Carlos, M. C. Ferro, J. F. Mano, P. Almeida, V. de Zea Bermudez, *RSC Advances* **2014**, *4 (103),* 59664–59675.
[7] P. Gomez-Romero, C. Sanchez, *Functional Hybrid Materials*, Wiley Interscience, New York, **2003**.
[8] C. Sanchez, B. Julián, P. Belleville, M. Popall, *J. Mater. Chem.* **2005**, *15*, 3559–3592.
[9] C. J. Brinker, G. W. Scherer, Sol-gel Science: *The Physics and Chemistry of Sol-Gel Processing*, Academic Press, San Diego, CA, **1990**.
[10] S. Mann, Biomineralization: Principles and Concepts in *Bioinorganic Materials Chemistry*, Oxford Chemistry Masters, Oxford University Press, **2001**.
[11] J. J. E. Moreau, L. Vellutini, M. Wong Chi Man, C. Bied, J. L. Bantignies, P. Dieudonné, J. L. Sauvajol, *J. Am. Chem. Soc.* **2001**, *123*, 7957–7958.
[12] E. Besson, A. Mehdi, C. Reye, P. Gaveau, R. J. P. Corriu, *Dalton Trans.* **2010**, *39*, 7534–7539.
[13] N. Liu, K. Yu, B. Smarsly, D. R. Dunphy, Y.-B. Jiang, C. J. Brinker, *J. Am. Chem. Soc.* **2002**, *124*, 14540–14541.
[14] L. D. Carlos, V. de Zea Bermudez, V. S. Amaral, S. C. Nunes, N. J. O. Silva, R. A. S. Ferreira, J. Rocha, C. V. Santilli, D. Ostrovskii, *Adv. Mater.* **2007**, *19*, 341–348.
[15] S. C. Nunes, N. J. O. Silva, J. Hummer, R. A. S. Ferreira, P. Almeida, L. D. Carlos, V. de Zea Bermudez, *RSC Adv.* **2012**, *2*, 2087–2099.
[16] G. Arrachart, G. Creff, H. Wadepohl, C. Blanc, C. Bonhomme, F. Babonneau, B. Alonso, J. L. Bantignies, C. Carcel, J. J. E. Moreau, P. Dieudonné, J.-L. Sauvajol, D. Massiot, M. Wong Chi Man, *Chem. Eur. J.* **2009**, *15*, 5002–5005.
[17] M. Fernandes, X. Cattoën, R. A. S. Ferreira, L. D. Carlos, M. Wong Chi Man, V. de Zea Bermudez, *J. Sol-Gel Sci. Tech.* **2013**, *65*, 61–73.
[18] H. Muramatsu, R. J. P. Corriu, B. Boury, *J. Am. Chem. Soc.* **2003**, *125*, 854–855.
[19] K. Okamoto, Y. Goto, S. Inagaki, *J. Mater. Chem.* **2005**, *15*, 4136–4140.
[20] J. Jiang, O. V. Lima, Y. Pei, X. C. Zeng, L. Tan, E. Forsythe, *J. Am. Chem. Soc.* **2009**, *131*, 900–901.
[21] B. Menaa, M. Takahashi, P. Innocenzi, T. Yoko, *Chem. Mater.* **2007**, *19*, 1946–1953.
[22] A. Chemtob, L. Ni, A. Demarest, C. Croutxe-Barghorn, L. Vidal, J. Brendle, S. Rigolet, *Langmuir* **2011**, *27*, 12621–12629.
[23] A. Shimojima, Y. Sugahara, K. Kuroda, *Bull. Chem. Soc. Jpn.* **1997**, *70*, 2847–2853.
[24] A. Shimojima, Y. Sugahara, K. Kuroda, *J. Am. Chem. Soc.* **1998**, *120*, 4528–4529.
[25] L. Ni, A. Chemtob, C. Croutxe-Barghorn, L. Vidal, J. Brendle, S. Rigolet, *J. Mater. Chem.* **2012**, *22*, 643–652.
[26] A. Shimojima, K. Kuroda, *Angew. Chem. Int. Ed.* **2003**, *42*, 4057–4060.
[27] A. Shimojima, Z. Liu, T. Ohsuna, O. Terasaki, K. Kuroda, *J. Am. Chem. Soc.* **2005**, *127*, 14108–14116.
[28] F. Lerouge, G. Cerveau, R. J. P. Corriu, *New J. Chem.* **2006**, *30*, 1364–1376.
[29] M. Fernandes, X. Cattoën, V. de Zea Bermudez, M. Wong Chi Man, *Cryst Eng Comm.* **2011**, *13*, 1410–1415.
[30] R. Besnard, J. Cambedouzou, G. Arrachart, O. Diat, S. Pellet-Rostaing, *Langmuir* **2013**, *29* (33), 10368–10375.
[31] R. Besnard, G. Arrachart, J. Cambedouzou, S. Pellet-Rostaing, *Langmuir* **2016**, *32* (18), 4624–4634.
[32] X. Cattoën, A. Noureddine, J. Croissant, N. Moitra, K Bürglová, J. Hodacová, O. de los Cobos, M. Lejeune, F. Rossignol, D. Toulemon, S. Bégin-Colin, B. P. Pichon, L. Raehm, J.-O. Durand, M. Wong Chi Man, *J. Sol-Gel. Sci. Technol.* **2014**, *70*, 245–253.
[33] S. C. Nunes, K. Bürglová, J. Hodačová, R. A. S. Ferreira, L. D. Carlos, P. Almeida, X. Cattoën, M. Wong Chi Man, V. de Zea Bermudez, *Eur. J. Inorg. Chem.* **2015**, *7*, 1218–1225.
[34] M. Meldal, C. W. Tornøe, *Chem. Rev.* **2008**, *108* (8), 2952–3015.
[35] H. C. Kolb, M. G. Finn, K. Barry Sharpless, *Angew. Chem. Int. Ed.* **2001**, *40* (11), 2004–2021.
[36] S. C. Nunes, J. Hummer, V. T. Freitas, R. A. S. Ferreira, L. D. Carlos, P. Almeida, V. de Zea Bermudez, *J. Mater. Chem. C* **2015**, *3*, 6844–6861.
[37] S. Monredon, C. Bonhomme, F. Ribot, F. Babonneau, *J. Sol-Gel Sci. Technol.* **2009**, *50*, 152–157.
[38] C. Yoshina-Ishii, T. Asefa, N. Coombs, M. J. MacLachlan, G. A. Ozin, *Chem. Commun.* **1999**, 2539–2540.
[39] E. Poli, E. Merino, U. Díaz, D. Brunel, A. Corma, *J. Phys. Chem. C* **2011**, *115*, 7573–7585.
[40] V. T. Freitas, L. Fu, A. M. Cojocariu, X. Cattoën, J. R. Bartlett, R. Le Parc, J.-L. Bantignies, M. Wong Chi Man, P. S. André, R. A. S. Ferreira, L. D. Carlos, *ACS Appl. Mater. Interfaces* **2015**, *7*, 8770–8778.
[41] J. Clauss, K. Schmidt-Rohr, A. Adam, C. Boeffel, H. W. Spiess, *Macromolecules* **1992**, *25*, 5208–5214.
[42] A. N. Parikh, M. A. Schivley, E. Koo, K. Seshadri, D. Aurentz, K. Mueller, D. L. Allara, *J. Am. Chem. Soc.* **1997**, *119*, 3135–3143.
[43] L.-Q. Wang, J. Liu, G. J. Exarhos, K. Y. Flaniga, R. Bordia, *J. Phys. Chem. B* **2000**, *104*, 2810–2816.
[44] W. L. Earl, D. L. Van der Hart, *Macromolecules* **1979**, *12*, 762–767.
[45] L. D. Carlos, V. de Zea Bermudez, R. A. S. Ferreira, L. Marques, M. Assunção, *Chem. Mater.* **1999**, *11*(3), 581–588.
[46] L. Fu, R. A. S. Ferreira, N. J. O. Silva, L. D. Carlos, V. de Zea Bermudez, J. Rocha, *Chem. Mater.* **2004**, *16*(8), 1507–1516.
[47] K. Dakmouche, C. V. Santilli, S. H. Pulcinelli, A. F. Craievich, *J. Phys. Chem. B* **1999**, *103*, 4937–4942.
[48] P. Dieudonné, M. Wong Chi Man, B. P. Pichon, L. Vellutini, J.-L. Bantignies, C. Blanc, G. Creff, S. Finet, J.-L. Sauvajol, C. Bied, J. J. E. Moreau, *Small* **2009**, *5(4),* 503–510.
[49] G. Creff, B. P. Pichon, C. Blanc, D. Maurin, J.-L. Sauvajol, C. Carcel, J. J. E. Moreau, P. Roy, J. R. Bartlett, M. Wong Chi Man, J.-L. Bantignies, *Langmuir* **2013**, *29 (18),* 5581–5588.
[50] A. M. Cojocariu, X. Cattoën, R. Le Parc, D. Maurin, C. Blanc, P. Dieudonné, J.-L. Bantignies, M. Wong Chi Man, J. R. Bartlett, *Phys. Chem. Chem. Phys.* **2016**, *18*, 7946–7955.
[51] K. Bürglová, N. Moitra, J. Hodačová, X. Cattoën, M. Wong Chi Man, *J. Org. Chem.* **2011**, *76,* 7326–7333.
[52] C. Boehm, F. Leveiller, D. Jacquemain, H. Mohwald, K. Kjaer, J. Als-Nielsen, I. Weissbuch, L. Leiserowitz, *Langmuir* **1994**, *10*, 830–836.
[53] S. S. Nobre, C. D. S. Brites, R. A. S. Ferreira, V. de Zea Bermudez, C. Carcel, J. J. E. Moreau, J. Rocha, M. Wong Chi Man, L. D. Carlos, *J. Mater. Chem.* **2008**, *18*, 4172–4182.
[54] S. C. Nunes, C. B. Ferreira, J. Hummer, R. A. S. Ferreira, L. D. Carlos, P. Almeida, V. de Zea Bermudez, *J. Mater. Chem. C* **2013**, *1*, 2290–2301.
[55] S. C. Nunes, R. A. S. Ferreira, L. D. Carlos, P. Almeida, V. de Zea Bermudez, *J Phys Chem B* **2013**, *117(46),* 14529–14543.
[56] M. D. Porter, T. B. Bright, D. L. Allara, C. E. D. Childsey, *J. Am. Chem Soc.* **1987**, *109*, 3559–3568.
[57] R. Wang, G. Baran, S. L. Wunder, *Langmuir*, **2000**, *16*, 6298–6305.
[58] N. V. Venkataram, S. Vasudevan, *J. Phys. Chem. B* **2001**, *105*, 7639–7650.
[59] N. V. Venkataram, S. Bhagyalakshmi, S. Vasudevan, R. Seshachi, *Phys. Chem. Chem. Phys.* **2002**, *4*, 4533–4538.
[60] S. Singh, J. Wegmann, K. Albert, K. Muller, *J. Phys Chem. B* **2002**, *106*, 878–883.
[61] R. G. Snyder, H. L. Strauss, C. A. Ellinger, *J. Phys. Chem.* **1982**, *86*, 5145–5250.
[62] K. G. Brown, E. Bicknell-Brown, M. Ladjadj, *J. Phys. Chem.* **1987**, *91*, 3436–3442.
[63] S. C. Nunes, V. de Zea Bermudez, J. Cybinska, R. A. S. Ferreira, J. Legendziewicz, L. D. Carlos, M. M. Silva, M. J. Smith, D. Ostrovskii, J. Rocha, *J. Mater. Chem.* **2005**, *15*, 3876–3886.
[64] L. D. Carlos, R. A. S. Ferreira, R. N. Pereira, M. Assunção, V. de Zea Bermudez, *J. Phys. Chem. B* **2004**, *108*, 14924–14932.
[65] L. Fu, R. A. S. Ferreira, N. J. O. Silva, L. D. Carlos, V. de Zea Bermudez, J. Rocha, *Chem. Mater.* **2004**, *16*, 1507–1516.

Submitted: November 23, 2016
Accepted: December 21, 2016